

The role of dust storms and aeolian dust deposition in the formation of Central European red clays and red paleosoils in loess sequences

PD108708 – financed by OTKA, Hungarian Research Council

Project closing final report

The research project OTKA PD108708 entitled 'The role of dust storms and aeolian dust deposition in the formation of Central European red clays and red paleosoils in loess sequences' officially ended on 31 December 2016, after a prolongation of 4 months (the project started on 1 September 2013).

The project was aimed at (1) determine the parent material of red clays and various paleosoils; (2) evaluate the interglacial dust sources, transportation pathways and sedimentation rate; (3) compare the development of red paleosoils of Carpathian Basin's loess series and Mediterranean "terra rossae"; and (4) increase the accuracy of geochemical climofunction by revealing the role of syngenetic fine-grained dust addition.

To achieve the above mentioned objectives a multi-proxy approach was used by simultaneous application of data from recent (modern observations, measurements and numerical simulations of Saharan dust events) and past (stratigraphic, sedimentary and geochemical data from dust deposits [Hungary; Slovakia; Croatia; Serbia; Italy]) sources. In the course of the project several drawbacks of the widely used laser diffraction measurements have been uncovered, and a brand new grain size and shape analysis technique have been introduced and developed (see the detailed description in the last part of report).

The results of the project were published in 6 peer-reviewed research papers (cumulative impact factor: 7.284) and in a book (in Hungarian); and were presented at major international conferences (DUST2014; Dan H. Yaalon Symposium; EGU2015; EGU2016; Loess2M). To reach a wider audience, results were also published in popular science magazine "Élet és Tudomány (Life and Science)". All details, events, scientific background and results of the project have been published at my homepages and blogs, at <http://porvihar.blogspot.hu/p/nkfi.html> and <http://aeoliandust.blogspot.hu/p/otka.html> and under OTKA tags.

Recent observations of aeolian dust deposition

[Publications: Varga et al., (2014a); Varga et al., (2014b); Varga et al., (2014c); Varga et al., (2016a)]

MED: Based on recent observations, measurements and numerical simulations, nowadays, the aeolian dust deposition has been governed by Saharan dust events in the study area (syngenetic aeolian accumulation of local clayey and silty material can be neglected). Investigations focused on Mediterranean areas indicated that Saharan dust accumulation had a pivotal role in the formation of red soil units in the Pliocene and during past interglacial periods of Pleistocene. To compare the modern (and assess the past interglacial) Saharan dust accumulation in the Mediterranean and in the Carpathian Basin, satellite measurements have

been used (for a consistent comparison, we applied the same methodology and database for the Mediterranean studies (Varga et al., 2014a), that we had used in our previous work in the Carpathian Basin (Varga et al., 2013)).

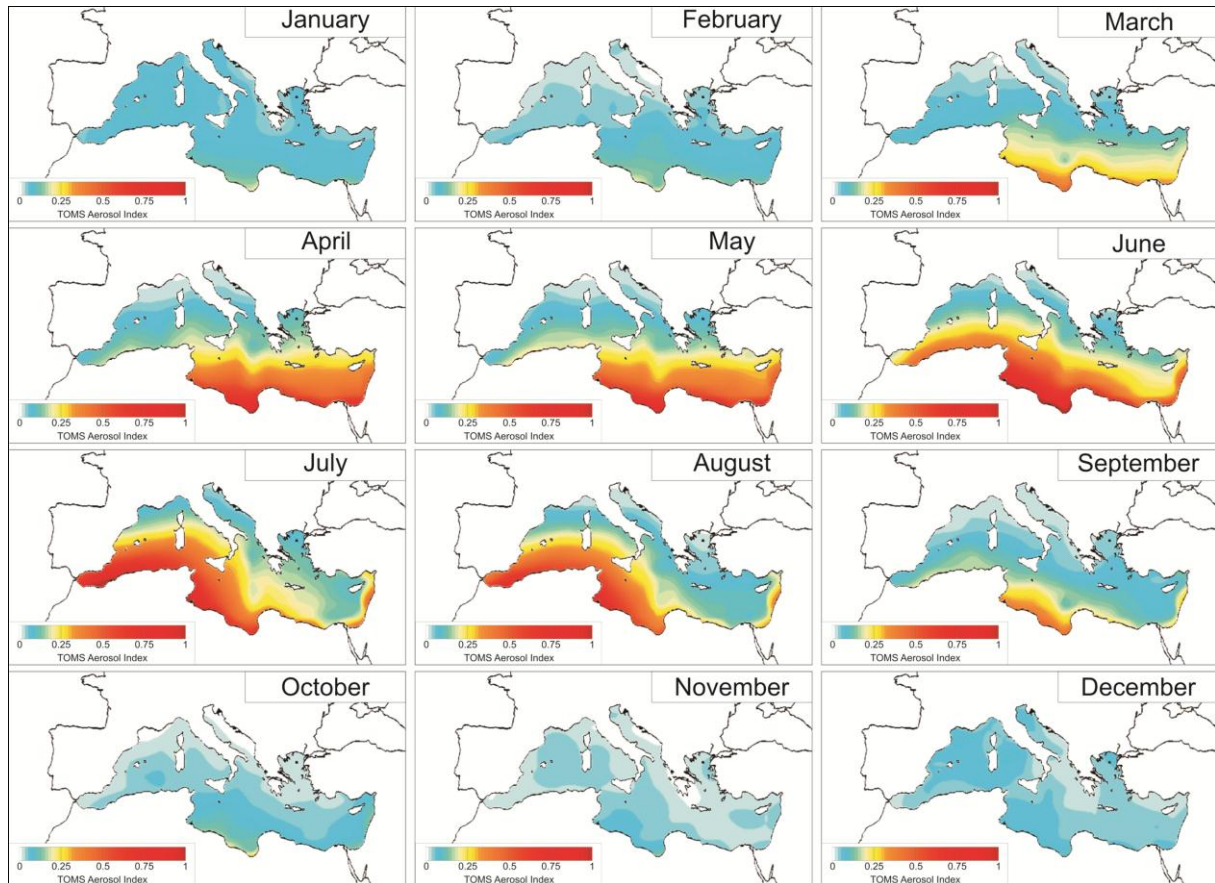


Fig.1. Compiled monthly mean aerosol maps of the Mediterranean study region (Varga et al., 2014a)

This study demonstrates that Saharan dust particles are essential components of the Mediterranean atmosphere, especially during spring and summer seasons. According to our systematic analysis of daily Aerosol Index data matrices, Saharan dust could be identified in 23.5% of all measurements in the Western basin (Alboran and Balearic Seas), in 29.5% in the Central Mediterranean (Tyrrhenian and Ionian Seas, Sea of Sicily) and in 33.75% in the Eastern Mediterranean. Two different types of synoptic situations are associated with Saharan dust outbreaks in the Mediterranean Basin. During spring mineral particles are carried on the foreside of eastward moving low-pressure systems, responsible for dust events in the Central and Eastern Mediterranean sub-basins. Summer dust episodes are found to be connected to the northward migration of the subtropical high-pressure belt. Regarding the formation of southward moving troughs in the Eastern Atlantic, strong SW flow transports dust towards the Western and Central Mediterranean regions. Depending on the different type of meteorological situations, different areas (with different geochemical fingerprints) could serve as dust source regions.

CB: In the Carpathian Basin four unusually severe Saharan dust episodes were analysed by a multi-proxy approach, using satellite measurements and images, computer simulations (Barcelona Supercomputing Center DREAM 8b v2.0 model), synoptic meteorological analyses, trajectory calculations, completed also with scanning electron microscopic (SEM) images and grain size measurements (Varga et al., 2014b). The effects (atmospheric diming; dry and wet deposition, etc.) of these episodes could also be observed by naked eyes. The investigated events were connected to steep pressure gradient between a western low pressure system and a blocking (south)easterly high; the exact location of these pressure centres could be slightly varied. Synoptic meteorological situations during the Central European dust episodes created enhanced meridionality leading to warm incursions in SE and E Europe, while western parts of the continent suffered from unseasonal cold weather. The most intense dust intrusions were results of southward expanding troughs over W Europe and NW Africa, which created cut-off lows, while one “blood rain” event was caused by a wide, stationary cyclone over Europe and a central Mediterranean dust intrusion generated by a shallow Sharav cyclone. The intensity of the discussed dust events was explained by the unusual stationary behaviour of major pressure systems and blocking mechanisms.

The grain size measurements of the deposited and collected Saharan dust material (with a 6.5 μm modal grain size) agree well with the separated fine-grained, “background dust” sedimentary populations of aeolian dust deposits in the Carpathian Basin. The SEM images of the settled dust material showed that many of quartz grains have irregular and angular shapes with sharp edges, breaks, stepped surfaces and conchoidal fractures, very similar to previously investigated fine-grained red clay and loess grains. These dust events were completed with the analyses of other unusually intense episodes from 2015 and 2016, which were discussed in detailed by Varga et al., 2016.

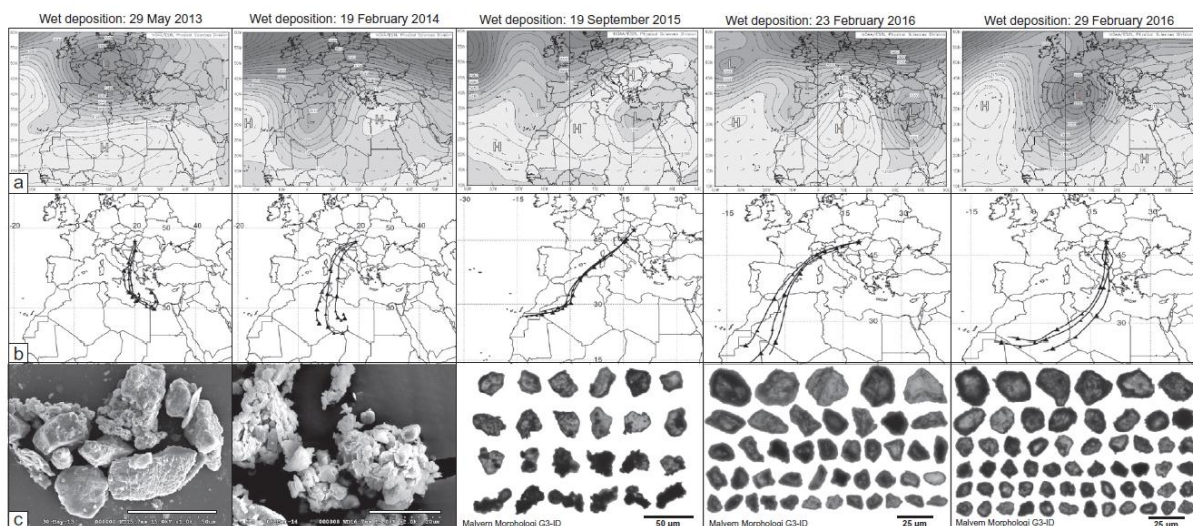


Fig.2. Intense Saharan dust depositional events in the Carpathian Basin (a: mean geopotential height and wind vectors at 700 hPa during the SDEs; b: trajectories of Saharan dust transportation; c: SEM micrographs and Malvern Morphologi G3-ID images of collected dust samples) (Varga et al., 2016a).

Past dust deposition: time-frame, geomorphology, environment

[Publications: Varga, (2015); Bradák et al., (2013); Bradák et al., (2014)]

Loess-paleosol sequences in Hungary (Central Europe) provide insight into the cyclic nature of glacial-interglacial variations of the last 1 million years. The paleosols have been recognized as the product of warmer and moister interglacials, when the (glacial) loess material was altered by chemical weathering and pedogenic processes. The gradual change from oldest red Mediterranean soils via forest and forest-steppe soils to steppe soils represents well the continuous decrease of chemical alteration of interglacial paleosols determined by environmental factors and duration of soil formation. The chronological subdivision of old paleosols is based on the controversial position of Matuyama-Brunhes Boundary (MIS-19), the only reference point, which was placed in the upper part of the PD2 soil (Sartori et al., 1999). However, the correlation of the thick, well-developed, rubefied PD1 paleosol with MIS-17 interglacial is unlikely. According to the studies of Basarin et al. (2014) and Buggle et al. (2014) MIS-17 is represented by the V-S6 fossil Cambisol in Serbia and its iron mineralogical proxies indicate lower temperature and/or more summer precipitation, an unsuitable condition for rubefied brown forest soil formation. Based on these considerations and a recently proposed Danube loess stratigraphic subdivision by Marković et al. (2015) the older red soils are equivalent to PD1: MIS-19; PD2: MIS-21 and PDK: MIS-25.

The loess deposits are generally underlain by the strata of the Tengelic Red Clay Formation, which age is Late Pliocene to Early Pleistocene, and is regarded as a thick paleosol complex, a series of B horizons. The lower, older member of this unit is rich in smectite, mixed-layer smectite/kaolinite and kaolinite, and was developed under a humid subtropical climate. The younger member of the red clay unit includes more fresh material (illite, chlorite) and was formed in a warm Mediterranean-like climate. Similar deposits are known from other sites of the region: Stari Slankamen – Serbia. The detailed granulometric analyses of the red clays show similarity in terms of their bimodal grain-size distribution patterns with loess horizons. Two main components can be distinguished from the curves. The coarse component (16–63 μm) has positive skewness and leptokurtic kurtosis, the material is well sorted; while the skewness of the fine-grained component (2–8 μm) is also positive, but the kurtosis is platykurtic, poorly sorted. More pronounced secondary maxima were identified in the case of Istrian and South Italian samples, while granulometry of Croatian and Serbian paleosol deposits were fairly similar to the Hungarian samples. The proportion of the fine-grained population is around 31–33% in the red clay samples, 24–25% in the paleosols, and 20–22% in the loess deposits. The Late Miocene deposits (conglomerates, sandstones, sands, clays) eroded from the Eastern Alps and the local Messinian sands could be the source material of the coarse sediment population of the red clays, while the background dust-load is represented in the fine component.

Climate-related paleoweathering conditions have been reflected in the major elemental geochemical composition of paleosol samples, and geochemical transfer functions can be applied to derive mean annual precipitation and mean annual temperature estimates. The quantitative assessment of climatic indicators relies on the selective removal of soluble and mobile elements from the soils compared to the relative enrichment of non-soluble elements.

Major element data of the sampled units were used as input of the paleoenvironment indicator geochemical transfer functions to quantify mean annual precipitation and temperature. These kinds of quantitative data on past climate and the stratigraphic data allow us to fit our pedostratigraphic units into a global context. The possibility of significant interglacial aeolian dust deposition is leading to several other questions. According to the classical assumption, the loess deposits have been formed from the depositing dust material, while the paleosoils developed from the underlying loess deposits by weak weathering processes. However, intensive interglacial dust accumulation claims a different kind of stratigraphic interpretation. In the first case, when the soils were formed from the underlying deposits, the last period of loess formation could not have been identified as loess layer in the sequence. In the second case, the soils form syngenetically from the falling dust, and all of the changes are represented in the stratigraphic column. From a paleoclimatic viewpoint, these glacial-interglacial shifts and abrupt warmings of glacial climax periods are one of the most interesting research topics.

The paleoprecipitation and paleotemperature data of the widely used geochemical climofunctions deserve also further reconsideration. The fine-grained populations of deposits are consisting of detrital and secondary particles; only the secondary ones provide relevant information on the environmental properties of the soil formation. By the assessment of the amount of detrital, windblown clay-minerals the result of these reconstructions could be refined significantly.

Possible role of aeolian dust deposition in the formation of interglacial soils

[Varga et al., (2016a)]

Past dust flux estimations are dependent on a reliable chronological framework and sedimentary features of aeolian dust deposits. The local and distant dust material as main sedimentary subpopulations are restored in the bimodal grain size distribution curves; these can be decomposed by using mathematical-statistical methods including parametric curve-fitting deconvolution and end-member modelling algorithms. These two populations of aeolian dust deposits are interpreted as the fine-grained continuous background dust-load of the atmosphere and the coarse-grained product of episodic dust storms, by analogy with grain size data of recent dust observations. The volumetric fraction of fine-grained component is ranging from 8.9% to 31.8%, but in most cases it is between 10% and 15%. Grain size of this sedimentary population is generally below 20 μm . Particle size characteristic of present-day Saharan dust is fairly diverse, but in most cases the dominant component of the transported material is clay and fine silt-sized fraction. The granulometric characteristic of fine-grained fractions of paleosoils and red clay samples were very similar to the collected Saharan dust material.

Sedimentation rate [m/y] is expressed as the quotient of loess thickness [m] and duration of loess formation [y], while the dust flux [$\text{g}/\text{m}^2/\text{y}$] is the product of sedimentation rate [m/y] and dry bulk density [kg/m^3]. The calculated total and background dust flux values (by using mass accumulation rates and grain size data) for glacial periods in the Carpathian Basin can be set into the range of 200 to 500 $\text{g}/\text{m}^2/\text{y}$ for total, and 25 to 60 $\text{g}/\text{m}^2/\text{y}$ for background dust

deposition, based on loess deposits (Újvári et al., 2010; Varga et al., 2012). It means, Saharan dust could represent a minor addition to the total amount of glacial loess deposits.

During interglacials, the local dust addition is assumed to have ceased (and the loess accumulation was terminated by the soil formation), at the same time the flux of far-travelled Saharan dust material is assessed by the estimated modern values of 3.2 to 5.4 g/m²/y and remained as a factor of aeolian sedimentation. Duration and intensity of interglacial soil forming periods were calculated from rescaled and standardized values of different global paleotemperature reference curves by Varga, (2015).

The total Saharan dust contribution to fine-grained population of soil material is the quotient of deposited Saharan dust material and soil mass of fine-grained population. Assuming that in the Pleistocene interglacials the dust deposition was in the same range as now a days (3.2 to 5.4 g/m²/y), the North African exotic dust material can represent 20-30% of clay and fine silt-sized components in the paleosoils.

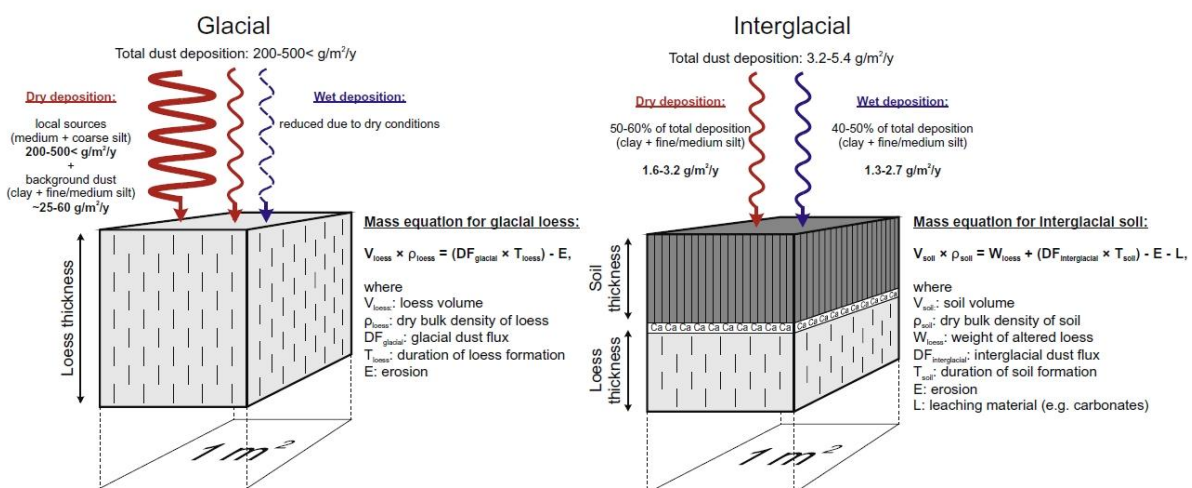


Fig.3. Schematic illustration of glacial and interglacial dust deposition mechanisms (Varga et al., 2016).

Calculations based on recent Saharan dust fluxes can be regarded as an average for Pleistocene interglacials, but the amount of emitted North African dust was higher during certain odd marine isotope stages. There are no proxies for past interglacial deposition in the Carpathian Basin, however, some information is available from the Eastern Mediterranean. By correlation of loess-paleosol series from Central Europe with sapropel sequences of the ODP967 marine core, it was visible that during the formation of the paleosoils, the Saharan dust flux was fairly weak, similar to the present-day conditions. However, around the Early-Middle Pleistocene transition dust emission from North Africa was also intense during interglacials and there was no sapropel formation in the Eastern Mediterranean. This period overlaps with the formation of red pedogene units in the Carpathian Basin.

The paleoenvironmental reconstructions and sedimentary data indicated that the formation of Early Pleistocene aeolian deposits was primarily determined by changes in the precipitation patterns rather than by glacial-interglacial variations (Varga, 2011). The climate of the Carpathian Basin in the MIS-19-21 warmer-moist periods was standing more under the

influence of the Mediterranean compared to later warm phases, which situation also more likely suggests meridional air-flow patterns and more frequent intrusions of Mediterranean cyclones. Relationship between Saharan dust intrusions and large-scale periodical variations (e.g. El Niño Southern Oscillation, North Atlantic Oscillation) is still controversial. However, intense dust emission periods have been simultaneous with major El Niño events according to Prospero and Lamb (2003). This could be an additional factor in the study of Pliocene red windblown dust deposits (e.g. red clays in the Carpathian Basin), because the time of their formation was determined as the so-called ‘El Padre’ global climate pattern, a permanent El Niño-like state (Ravelo et al., 2006; Shukla et al., 2009).

Higher amount of transported and deposited Saharan dust material in the Pliocene is also supported by modern observations by Varga et al. (2014b) and Varga et al. (2016a). The reported synoptic meteorological background of very intense dust episodes were determined by the unusually stationary behaviour of pressure centres and exceptional meridional flow patterns. According to the studies of Francis and Vavrus (2012), the weaker equator-to-pole temperature gradient due to intense warming of polar regions (known as arctic or polar amplification) contribute to a slower eastward progression of Rossby waves, leading to increasing wave amplitudes and enhanced flow meridionality. During Pliocene – which period also offers an opportunity to understand a warmer-than-present world – the polar regions were more warmer and the difference between high and low latitude areas was reduced (Brigham-Grette et al., 2013), suggesting a more dominant role of meridional atmospheric flow patterns.

Development of a new methodological procedure in granulometry of aeolian dust and dust deposits

[Conference presentations: Varga et al., (2015a); Varga et al., (2015b); Varga et al., (2016b); Varga et al., (2016c)]

The results of the development and application of new granulometric investigations have not yet been published in research journals, but the preliminary results were presented on international conferences (Varga et al., 2015, 2016b, 2016c). The research paper ‘*Granulometric properties of aeolian dust deposits: what are we measuring?*’ (working title) is in preparatory and it will be submitted to Q1/D1 scientific journal.

As this part of the project has not yet been discussed in detail in publications, the results will be introduced in the next pages of the report.

Introduction

Determination of granulometric parameters is standing in the focal point of sedimentary studies and it is of growing interest in the Earth sciences. Particle size data of sedimentary deposits provide insights into the physicochemical environment of entrainment, transport, accumulation and post-depositional alterations of sedimentary particles, and are important

proxies applied in paleoclimatic reconstructions. It is especially true for aeolian dust deposits with a fairly narrow grain size range as a consequence of extremely selective nature of sediment transport by wind. Therefore, various aspects of aeolian sedimentation (wind strength, distance to source area or possible further source regions and modes of sedimentation and transport) can be reconstructed only from accurate grain size data via a correct sedimentary and paleoclimatic interpretation.

Grain size distribution data obtained from the most widely used particle sizing technique, the laser light scattering measurement provides information on the volumetric amount of particles arranged into ca. 100 size bins ranging from hundreds of nanometres up to several millimetres in size. However, laser scattering particle size data is indirect information on the sphere equivalent diameter of the particle; the light scattering pattern of the measurements must be transformed by different optical models (Fraunhofer and Mie theories) to attain particle size distribution data.

Not only size, but shape parameters of particles are holding vital information on sedimentary mechanisms (transport and deposition) and post-depositional, environment-related alterations. Automated static imaging was applied to gather direct information on particle size and shape parameters. Image analysis techniques have been applied widely, however previously published studies were carried out on populations with much smaller number of particles. The average particle number of automated imaging measurements is ca. 10^4 - 10^6 particles, which provide us to gain a statistically robust and objective insight into the morphological characteristics of the particles. Various size and shape parameters, as well as optical intensity values of each particle are measured routinely and the number based results are converted to volumetric distributions, so the direct comparison of the results with laser diffraction data is easily feasible. To date, there has been very few data published on automated image analyses of size and shape parameters of sedimentary deposits, so much uncertainty exists about the relationship between the different applied methods.

Material

Samples were collected from key-sites of the Carpathian Basin (Hungary; Croatia; Serbia) with a special attention to the diverse paleosoil members. Soil material were taken from marker pedogene units (MIS-5 to MIS-21) and red clays, while the loess samples were gathered also from young, last glacial (MIS-2) and old, late Lower Pleistocene (MIS-20) strata to investigate the deposits both of the onset and the termination of loess formation in the area.

XRD measurements indicate that quartz (~30-60%), 10Å phases (illite±muscovite±biotite: 20-30% in loess and 10-20% in paleosoil), carbonates and 14Å phases (smectite±vermiculite±chlorite) are the dominant. Bulk mineral composition data served as basis for optical settings of laser diffraction measurements. Reported refractive indices of loess and soil-forming minerals generally fall within a relatively narrow range, however, the value of absorption coefficient is dependent also on particle shape and surface roughness beside the mineralogical composition. In order to get an overview on particles size distributions and on effects of optical settings, calculations were made with the combination of various refractive indices (1.45-1.6) and absorption coefficients (0.01-1).

Laser light scattering measurements

Laser light scattering particle sizing technique is an indirect estimation of grain size distribution by measuring the angular variation in intensity of light scattered (diffracted, refracted and reflected) and absorbed, as a laser beam passes through a dispersed particulate sample. Grain size distributions of loess and paleosol samples were analysed using three different instruments: Fritsch Analysette 22 Microtec Plus (Fritsch); Horiba Partica La-950 v2 (Horiba) and Malvern Mastersizer 3000 with a Hydro Lv wet dispersion unit (Malvern). Particle size data are determined as volume percentage of particles classed into ~100 logarithmically distributed size bins from several nanometres to millimetres (Fritsch: 0.08-2000 μm [108 size bins]; Horiba: 0.01-3000 μm [93 size bins]; Malvern: 0.01-3000 μm [101 size bins]). Laser light scattering patterns of two light sources (Fritsch: IR 850 nm; green 532 nm; Horiba: red 650 nm; blue LED 405 nm; Malvern: red 633 nm; blue LED: 470 nm) were measured by focal plane detectors, side and backward scattered light detectors.

Automated static image analysis procedure

Automated imaging provides a unique technique to gather direct information on granulometric characteristics of particles. Granulometric data obtained from automatic image analysis of Malvern Morphologi G3-ID is a rarely applied new technique for particle size and shape analyses in sedimentary geology. Sedimentary particles are dispersed with an instantaneous pulse of compressed air onto a flat glass to consistently orienting them with their largest area facing to the camera. In contrast during laser diffraction measurements, the random orientation of some lamellar shaped clay minerals could lead to a significant underestimation of grain size. Size and shape data of 10^4 - 10^6 individual particles are automatically recorded for each sample from the captured high-resolution images. Several size (e.g. circle-equivalent diameter, major axis, length, width, area) and shape parameters (e.g. elongation, circularity, convexity) are calculated by the instrument software. At the same time the mean light intensity measured after transmission through each particle is automatically recorded by the system as a proxy of optical properties of the material providing further information. Mean intensity values are dependent on chemical composition and/or thickness of the particles, while standard deviations of intensities are linked to heterogeneity of particle constitution and surface morphology.

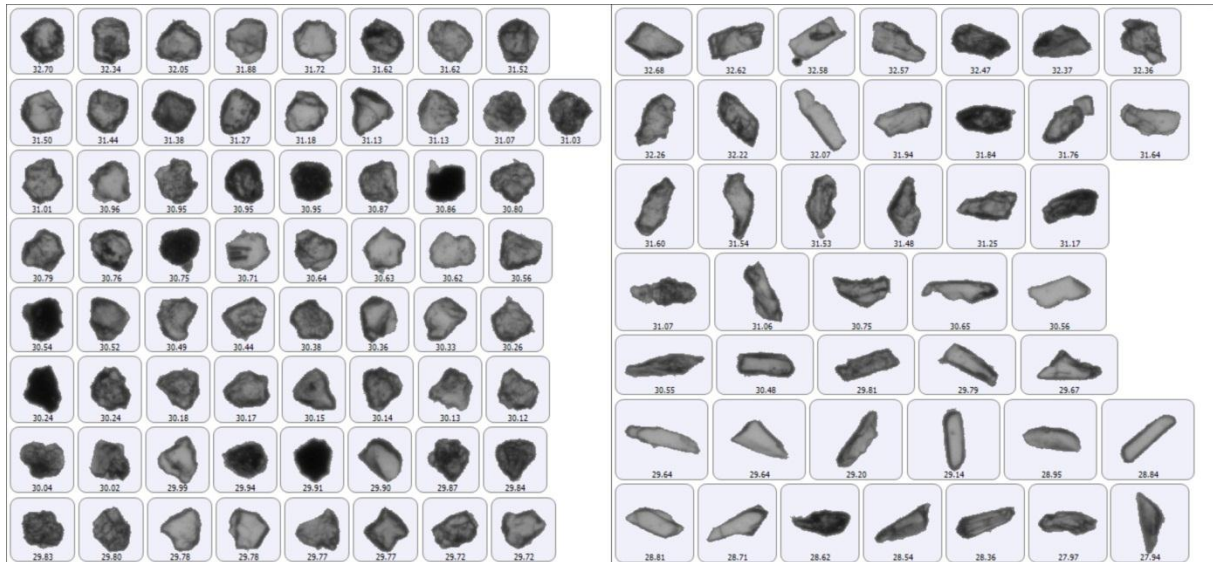


Fig.4. Malvern Morphologi G3-ID images of paleosol particles with similar circle-equivalent (CE) diameter, but various circularity parameters.

Image analysis-based measurements are organized into a number-based database. All of the particles have their own identity number (ID), which is the primary key in the data matrix. Each row represents one particle and the columns of the table are the size and shape parameters. The large number of measured particles ensures the statistically robust and objective insight into the granulometric characteristics of the samples. To get a grain size distribution, the individual CE diameter data are classified into grain size bins (to make the comparison easier and more representative, we used the logarithmic size bins of the laser diffraction measurements). The number-based distribution curves can be converted easily into volume- or surface area-weighted distributions by using the central values of size bins as diameters.

Scanning electron microscopy

Scanning electron microscopy uses a focused beam of electrons to form magnified images which are high contrast and extremely sharp suitable for particle surface morphology characterization. Size and shape of individual particles can be accurately assessed by image analysis software and it is considered as a direct and absolute measure of particle size. The main drawback of this method is the relatively small population of analysed particles (a few hundred).

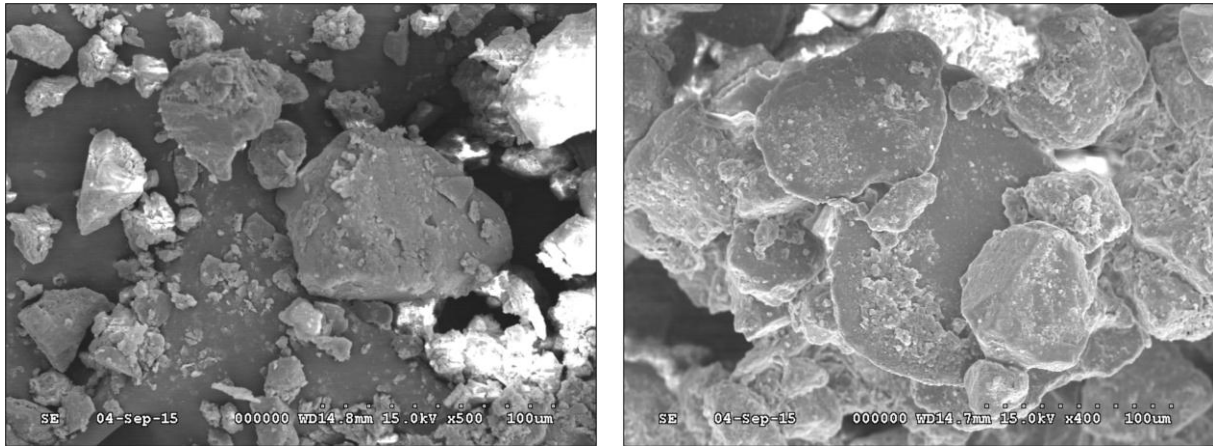


Fig.5. SEM micrographs of silt-sized particles from paleosoil samples.

Results

Laser scattering measurements show that the majority of mineral particles of the samples fall into silt ranges with minor clay and very fine sand components. All of the loess grain size distribution curves have fairly similar, uniform shape patterns with definite positive skewness (asymmetry into the direction of coarse fractions), unimodality (or weakly developed bimodality) and leptokurtic kurtosis. The pronounced maximum in medium and coarse silt fraction and a tail or shoulder in the clay and fine silt components indicate a primary aeolian depositional environment. Paleosoils have more complex granulometric profile with slightly lower mean and modal grain size, higher clay-content, slightly modest kurtosis and a more distinct clay/fine silt shoulder compared to underlying loess.

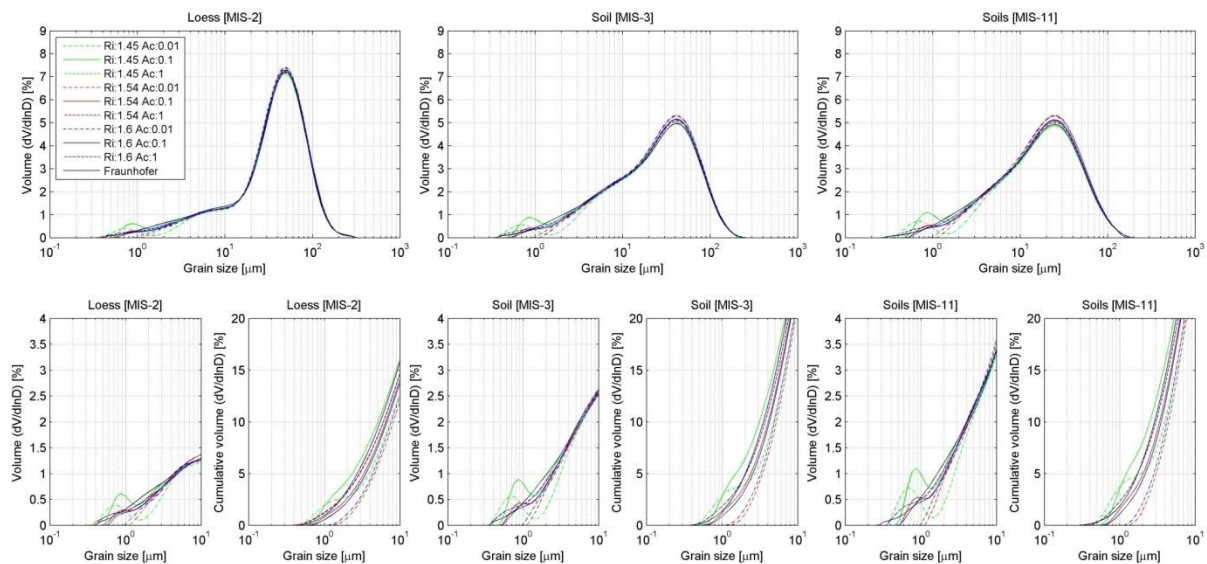


Fig.6. Grain size distributions of different samples and detailed analyses of fine-grained fractions.

The differences of various settings are clearly visible in case of finer size fractions, but there are no significant differences in the medium and coarse silt content (therefore it has minor effect on the mode of distribution curves). Optical setting changes are able to create an additional maximum in the submicron fractions, which lead to an increase in the clay-sized

fraction. The separate effects of various refractive index (Ri) and absorption coefficient (Ac) settings were also analysed. In the case of the Ri effect analyses, the Ac values were held constant at 0.01, 0.1 and 1, while Ri values were varied between 1.45 and 1.6. The Ri settings significantly affected the grain size distribution, particularly $Ri < 1.5$; however Ri effect was less pronounced in the case of higher values, which are leading to an almost constant clay content after a persistent decrease. In order to analyze the effect of Ac settings the Ri value was held constant at 1.54, and the Ac values were varied between 0.01 and 1 (from almost transparent to totally opaque). While the Ri values of most soil-forming minerals can be found in the literature, their Ac values are neither available nor cannot be measured precisely in case of relatively small particles (e.g. clay minerals).

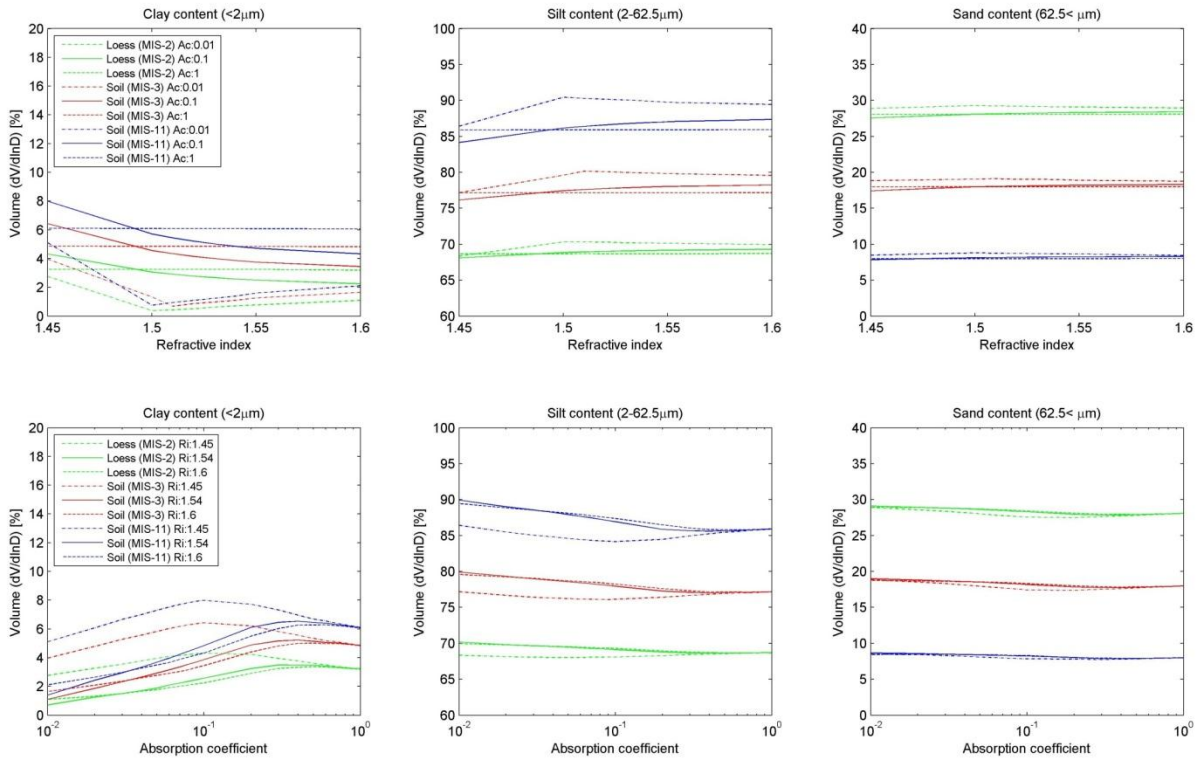


Fig.7. Analyses of separate effects of refractive indices and absorption coefficients on grain size fractions.

Image analysis grain size results have indicated underestimation of clay and fine silt fractions compared to laser diffraction measurements. The measured CE diameter of image analysis is calculated from the acquired two-dimensional image of the particle. It is assumed that the instantaneous pulse of compressed air disperses the sedimentary particles onto the glass slide with a consistent orientation with their largest area facing the camera. However, this is only one outcome of infinite possible projections of a three-dimensional object and it cannot be regarded as a representative one. To demonstrate and quantify this distortion, we have made calculations with randomly rotated (simple) three-dimensional geometric solids. It is visible that onto XY-plane projected areas are dependent on two major factors: (1) rotation angles (α_x ; α_y); and (2) shape parameters (edge-ratios) of the objects. To determine the effect of rotation angles on projected areas, the α_x and α_y angles were modified from 0° to 179° and the projected areas were calculated for every rotation angle-pairs. The mean value of the rotation-

dependent XY-plane projected areas represents the orientation-averaged projected area of a random oriented object.

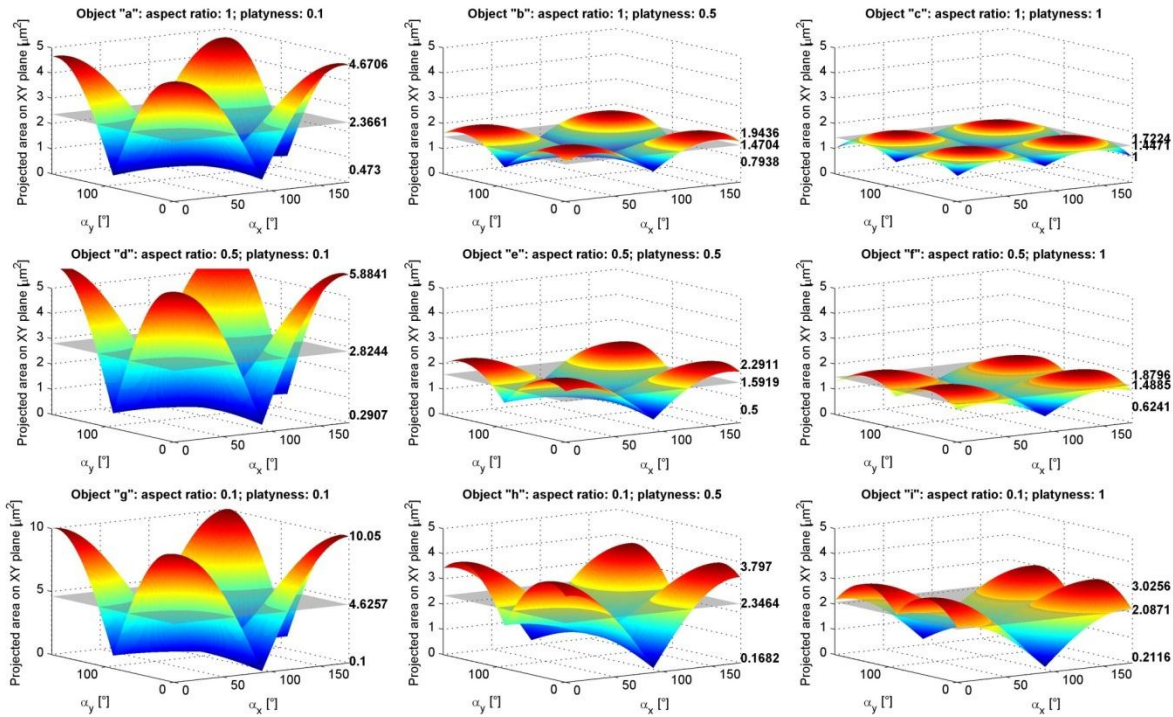


Fig. 8. Modelled rotation-averaged projected areas of simple 3D-objects.

Shape parameters of the solids were quantified based on the edge-ratios. Platyness (z/y) and aspect ratios (y/x) were chosen from 0.1 to 1 (0.1; 0.5 and 1 combinations are presented here at Fig.6. and Table 1.), while the volume of the solids was a constant $1 \mu\text{m}^3$. The introduced CE_{rot} ratio is the quotient of the largest face area-based CE diameter (it is assumed during the image analysis that this arbitrary configuration “represents” the particle) and orientation-averaged projected area-based CE diameter (as the projected area of a random oriented particle). The displayed surface shows the level of overestimation as a function of shape parameters (orientation-averaged projected area). Another weighting factor, the so-called CE/SE ratio was also introduced to reduce the inaccuracy of exchange transformation from number- to volume-based distribution functions. Aspect ratio of every single particle is known, which allowed us to get a more accurate 2-dimensional representation of 3-dimensional particles, so the platyness-averaged CE_{rot} and CE/SE correction factors were possible to determine.

Table 1. General characteristics and weighing factors of simple 3D-objects.

ID	Shape parameters		Edge lengths			Volume	Largest face		Projected areas on XY plane								CE_{rot} ratio	CE/SE ratio	
									Areas				CE diameters						
	Aspect ratio (y/x)	Platyness (z/y)	x	y	z	$[\mu\text{m}^3]$	SE diameter	Area	CE diameter	min	max	mean	std	min	max	mean			std
a	1	0.1	2.15	2.15	0.22	1	1.24	4.64	2.43	0.47	4.67	2.37	1.26	0.78	2.44	1.74	0.48	1.40	1.96
b	1	0.5	1.26	1.26	0.63	1	1.24	1.59	1.42	0.79	1.94	1.47	0.32	1.01	1.57	1.37	0.16	1.04	1.15
c	1	1	1.00	1.00	1.00	1	1.24	1.00	1.13	1.00	1.72	1.45	0.18	1.13	1.48	1.36	0.09	0.83	0.91
d	0.5	0.1	3.42	1.71	0.17	1	1.24	5.85	2.73	0.29	5.88	2.82	1.65	0.61	2.74	1.90	0.59	1.44	2.20
e	0.5	0.5	2.00	1.00	0.50	1	1.24	2.00	1.60	0.50	2.29	1.59	0.51	0.80	1.71	1.42	0.25	1.12	1.29
f	0.5	1	1.59	0.79	0.79	1	1.24	1.26	1.27	0.62	1.88	1.49	0.34	0.89	1.55	1.38	0.17	0.92	1.02
g	0.1	0.1	10.00	1.00	0.10	1	1.24	10.00	3.57	0.10	10.05	4.63	2.90	0.36	3.58	2.43	0.84	1.47	2.88
h	0.1	0.5	5.85	0.58	0.29	1	1.24	3.42	2.09	0.17	3.80	2.35	1.04	0.46	2.20	1.73	0.44	1.21	1.68
i	0.1	1	4.64	0.46	0.46	1	1.24	2.15	1.66	0.21	3.03	2.09	0.80	0.52	1.96	1.63	0.37	1.02	1.34

References

- Basarin, B., Buggle, B., Hambach, U., Marković, S.B., O'Hara Dhand, K., Kovačević, A., Stevens, T., Guo, Z., Lukić, T. (2014). Time-scale and astronomical forcing of Serbian loess–paleosoil sequences. *Global Planetary Change* 122: 89-106.
- Buggle, B., Hambach, U., Müller, K., Zöller, L., Marković, S.B., Glaser, B. (2014). Iron mineralogical proxies and Quaternary climate change in SE-European loess–paleosoil sequences. *Catena* 117: 4-22.
- Bradák B; Kiss K; Barta G; Varga Gy; Szeberényi J; Novothny Á; Szalai Z; Mészáros E; Markó A (2013). Lokális talajváltozatok a verőcei téglagyár környezetében: a Pécsi-féle löszrétge tan nyitott kérdései, *Földrajzi Közlemények* 137 (3): 312-322.
- Bradák, B., Kiss, K., Barta, G., Varga, Gy., Szeberényi, J., Józsa, S., Novothny, Á., Kovács, J., Markó, A., Mészáros, E., Szalai, Z. (2014). Different paleoenvironments of Late Pleistocene age identified in Verőce outcrop, Hungary: Preliminary results. *Quaternary International* 319: 119–136.
- Brigham-Grette J., Melles M., Minyuk P., Andreev A., Tarasov P., DeConto R., Koenig S., Nowaczyk N., Wennrich V., Rosén P., Haltia E., Cook T., Gebhardt C., Meyer-Jacob C., Snyder J., Herzschuh U. (2013): Pliocene warmth, polar amplification, and stepped Pleistocene cooling recorded in NE Arctic Russia. *Science*, 340: 1421-1427.
- Francis, J. A., S. J. Vavrus (2012), Evidence linking Arctic amplification to extreme weather in mid-latitudes, *Geophysical Research Letters*, 39, L06801
- Marković, S.B., Stevens, T., Kukla, G.J., Hambach, U., Fitzsimmons, K.E., Gibbard, P., Buggle, B., Zech, M., Guo, Z., Hao, Q., Wu, H., O'Hara Dhand, K., Smalley, I.J., Újvári, G., Sümegi, P., Timar-Gabor, A., Veres, D., Sirocko, F., Vasiljević, D.A., Jary, Z., Svensson, A., Jović, V., Lehmkuhl, F., Kovács, J., Svirčev, Z. (2015). Danube loess stratigraphy — Towards a pan-European loess stratigraphic model. *Earth-Science Reviews*, 148: 228-258.
- Ravelo, C.A., Dekens, S.P., McCarthy, M. (2006). Evidence for El Niño-like conditions during the Pliocene. *GSA Today*, 16: 4-11.
- Sartori, M., Heller, F., Forster, T., Borkovec, M., Hamann, J., Vincent, E. (1999). Magnetic properties of loess grain size fractions from the section at Paks (Hungary). *Physics of the Earth and Planetary Interiors*, 116: 53-64.
- Shukla, S.P., Chandler, M.A., Jonas, J., Sohl, L.E., Mankoff, K., Dowsett, H. (2009). Impact of permanent El Niño (El Padre) and Indian Ocean Dipole in warm Pliocene climates. *Paleoceanography* 24.
- Újvári, G., Kovács, J., Varga, Gy., Raucsik, B., Marković, S.B. (2010). Dust flux estimates for the Last Glacial Period in East Central Europe based on terrestrial records of loess deposits: a review. *Quaternary Science Reviews* 29: 3157-3166.
- Varga, Gy. (2011). Similarities among the Plio–Pleistocene terrestrial aeolian dust deposits in the world and in Hungary. *Quaternary International* 234: 98-108.

- Varga, Gy., Kovács, J., Újvári, G. (2012). Late Pleistocene variations of the background aeolian dust concentration in the Carpathian Basin: an estimate using decomposition of grain-size distribution curves of loess deposits. *Netherlands Journal of Geosciences – Geologie en Mijnbouw* 91: 159-171.
- Varga, Gy., Kovács, J., Újvári, G. (2013) Analysis of Saharan dust intrusions into the Carpathian Basin (Central Europe) over the period of 1979-2011. *Global and Planetary Change* 100: 333-342.
- Varga, Gy., Újvári, G., Kovács, J. (2014a). Spatiotemporal patterns of Saharan dust outbreaks in the Mediterranean Basin. *Aeolian Research* 15: 151-160.
- Varga, Gy., Cserhádi Cs., Kovács, J., Szeberényi, J., Bradák, B. (2014b). Unusual Saharan dust events in the Central European Carpathian Basin in 2013 and early 2014. *Weather* 69: 309-313.
- Varga, Gy., Bradák, B., Szeberényi, J. (2014c). Geographical distribution and geomorphological characteristics of major global dust source areas. In: Jakab, G., Szalai, Z. (Eds.) *Talajpusztulás térben és időben: az "Eróziós kerekasztal 2013" közleményei*: 40-46.
- Varga, Gy. (2015). Changing nature of pleistocene interglacials – is it recorded by paleosoils in Hungary (Central Europe)? *Hungarian Geographical Bulletin* 64: 313-322.
- Varga, Gy., Újvári, G., Kovács, J., Szalai, Z. (2015a). Effects of particle optical properties on grain size measurements of aeolian dust deposits. *Geophysical Research Abstracts*, Vol. 17. EGU2015-9848-1 EGU General Assembly 2015.
- Varga Gy.; Kovács J.; Szalai Z.; Újvári G. (2015b). Granulometric properties of aeolian dust deposits in the Carpathian Basin, *Hungarian Geographical Society (szerk.) EUGEO Budapest 2015: congress programme and abstracts*. 263 p.
- Varga, Gy., Cserhádi, Cs., Kovács, J., Szalai, Z. (2016a). Saharan dust deposition in the Carpathian Basin and its possible effects on interglacial soil formation. *Aeolian Research*: 1-12.
- Varga, Gy., Újvári, G., Kovács, J., Jakab, G., Kiss, K., Szalai, Z. (2016b). Granulometric profiling of aeolian dust deposits by automated image analysis. *Geophysical Research Abstracts*, Vol. 18. EGU2016-5512-2. EGU General Assembly 2016.
- Varga, Gy., Újvári, G., Kovács, J., Szalai, Z. (2016c). Granulometric properties of aeolian dust deposits: what are we measuring? IN: Marković, S.B. (Ed.) *Loess2M: Modelling and Mapping*. Abstract Book. pp. 50-51. (Loess2M - International Conference on Loess Research, Novi Sad, Serbia).